Influence of Ship-to-Ship Interaction on Formation Control of Multi-Vessel Systems

Xin Xiong[a], Rudy R. Negenborn[b] and Yusong Pang[c]
Department of Maritime and Transport Technology, Delft University of Technology, Delft, The Netherlands

Keywords: Formation Control, Multi-Vessel Systems, Ship-to-Ship Interaction.

Abstract: The formation control of autonomous surface vessels (ASVs) has received increasing attention, with research focusing on the formation generation and maintenance. However, the majority of existing researches neglect the effects of ship-to-ship interactions. Considering that in some scenarios, the distance between ships in a formation is small, it is necessary to conduct relevant research on formation control. Based on existing literature on ship hydrodynamic effects, this paper proposes a semi-empirical formula to describe the ship-to-ship interaction forces, with the main factors being the relative distance and velocity between ships. Subsequently, experiments were designed to independently analyze these two influencing factors, and control simulations were executed for a formation consisting of two homogeneous ASV. The simulation outcomes demonstrate that ship-to-ship interaction forces indeed influence control performance, with control performance errors directly correlating with the variations in interaction forces between the two ASV. Among these factors, speed exerts a greater influence than distance, rendering it challenging for a conventional PID controller to satisfy the stringent control requirements.

1 INTRODUCTION

In recent years, with the escalating complexity of maritime transport tasks and the increased variability of marine environments, a single Autonomous Surface Vessel (ASV) may prove insufficient to satisfy all operational demands (Negenborn et al., 2023)(Xiong et al., 2015). The cooperation of ASVs enables the execution of more intricate tasks and scenarios, thereby enhancing the overall efficiency of the waterborne transportation system (Chen et al., 2021). Furthermore, the deployment of ASVs can enhance the system's reliability and redundancy, also significantly fortifies the system's fault tolerance and operational continuity. Meanwhile, with the increasing of the number of controlled ASVs, the cooperation also encounter numerous challenges, particularly in the realm of cooperative control (Peng et al., 2020b; Du et al., 2021a; Oh et al., 2015).

In the domain of cooperative control, formation control represents a pivotal branch that concentrates on maintaining prescribed geometric configurations and relative positioning among ASVs engaged in collective task execution (Liu et al., 2023). In the existing literature, Various formation control methodologies have been explored, such as the leader-follower approach (Park and Yoo, 2018; Wang et al., 2022), behavioral approach (Tan et al., 2023; Qin et al., 2017), and virtual structure approach (Mu et al., 2020; Zhou et al., 2020), along with strategies including consensus-based (Peng et al., 2020a; Gu et al., 2019), relation-based (Liu et al., 2018), and position-based methods (Liu et al., 2022; Liu et al., 2017). Meanwhile, there are also some literature that investigate collision avoidance in formation control (Mondal et al., 2017; He et al., 2019), as well as controller design under environmental disturbances (Du et al., 2021b). However, most studies overlook the ship-to-ship interaction within the formation. In some formation scenarios, ships are close to each other, where ship-to-ship interaction significantly impact ship motions. Overlooking this hydrodynamic effect can result in diminished control performance or potentially lead to control failures (He et al., 2021).

The maneuvering characteristics of a single ASV are significantly influenced by hydrodynamic effects, with hydrodynamic coefficients of the ASV undergoing changes in response to variations in speed and en-

[a] https://orcid.org/0009-0009-7265-5077
[b] https://orcid.org/0000-0001-9784-1225
[c] https://orcid.org/0000-0001-8094-3436

Xiong, X., Negenborn, R. and Pang, Y.
Influence of Ship-to-Ship Interaction on Formation Control of Multi-Vessel Systems.
DOI: 10.5220/0012911700003822

In *Proceedings of the 21st International Conference on Informatics in Control, Automation and Robotics (ICINCO 2024) - Volume 1*, pages 25-36
ISBN: 978-989-758-717-7; ISSN: 2184-2809

vironmental conditions (Skjetne et al., 2004). Hydrodynamic interaction of multi ships under different situations have been analyzed, including ships in the process of lightering operation (De Decker, 2006; Sano and Yasukawa, 2019), overtaking and encounters (Chen et al., 2019; Setiawan and Muin, 2018; Yu et al., 2019). These finds indicate that when two ships are in close proximity, phenomena such as "bow repulsion" and "bow attraction" occur. These are due to the changes in interaction forces between the ships. Thus it is essential to further investigate the influence of ship-to-ship interactions on formation control.

The methods for investigating ship-ship interaction can generally be categorized into three types: First, physical model testing, which entails the use of scaled model ships within towing tanks (Lataire et al., 2011; Lataire et al., 2009). This method has high precision and can accurately reflect the behavior of ships, but it is costly, time-consuming, and has issues with scale effects; Second, numerical simulation, employing Computational Fluid Dynamics (CFD) or potential flow panel methods to simulate hydrodynamic interactions under specific conditions-a method favored for its high flexibility and cost -effectiveness (Wnęk et al., 2018; Yuan et al., 2016; He et al., 2022); Third, theoretical analysis and empirical model development, involving the derivation of empirical formulas from experimental data to model hydrodynamic effects (Varyani et al., 2002; Vantorre et al., 2002; Dong et al., 2022). This method enables rapid prediction of changes in hydrodynamic effects, rendering it well-suited for addressing real-time control. It is also cost-effective and easy to use; therefore, this paper employed this method to model ship-ship interaction.

This paper focuses on the influence of the ship-ship interaction on formation control. By summarizing and processing formulas and data from existing literature, a semi-empirical formula suitable for control system was proposed to describe these variations, which was applied to formation control. Subsequently, relevant formation control simulations can be conducted to investigate the impact of the factors of formulas on formation control.

This paper is organized as follow. In Section 2, we establish models for the formation system, including the kinematic model of the ASV and the ship-to-ship interaction model. In the Section 3, we define some parameters required for the simulation experiments and refined the Tito-Neri kinematic model. Then, we design simulation experiments focusing on two important factors: speed and distance. The results of simulation experiments are provided in Section 4 to demonstrate the influence of the ship-to-ship interaction of control, followed by the analysis and explanation. Finally, conclusions and future research directions are given in Section 5.

2 ASVs SYSTEM MODELING

2.1 ASV Motion Model

An ASV is a complex system characterized by large inertia and time-delay properties. To establish the motion model of ASV is the foundational task for formation control. This paper primarily focuses on underactuated ASV as shown in Fig. 1, with the system input consisting of two degrees of freedom, namely thrust and torque $\tau = [\tau_u \ \ \tau_r]^T$. The plane motion of a vessel can be described by the 3-DOF (degree of freedom) kinematics and kinetics model which is widely called Fossen model (Fossen, 2011), which is expressed as:

$$\begin{aligned}\dot{x} &= f(x_R, u_R) \\ &= M_{RB}\dot{v} + M_A\dot{v} + C(v(t))\,v(t) + D(v(t))\,v(t) = \tau(t)\end{aligned} \tag{1}$$

$$\dot{\eta}(t) = R(\psi(t))\,v(t), \tag{2}$$

Where $x = [x\ y\ \psi\ u\ v\ r]^T$ as the system's state variable, $\dot{\eta}(t) = (x, y, \psi)$ is the position vector in the world frame and the heading. $v(t) = [u(t)\ v(t)\ r(t)]^T \ \varepsilon\, \mathbb{R}^3$ is the velocity vector in the Body-fixed frame containing the velocity of surge $u(t)$,sway $v(t)$, and yaw $r(t)$. The terms $M \in \mathbb{R}^{3\times3}$, $C \in \mathbb{R}^{3\times3}$,$D \in \mathbb{R}^{3\times3}$ are the Mass (inertia), Coriolis-Centripetal, and Damping matrix, respectively. $u = \tau' = [\tau_u\ ,\ \tau_r]^T$ as the system's control input, $R\varepsilon\mathbb{R}^{3\times3}$ is the standard rotation matrix, which is defined as:

$$R(\psi(t)) = \begin{bmatrix} cos(\psi(t)) & -sin(\psi(t)) & 0 \\ sin(\psi(t)) & cos(\psi(t)) & 0 \\ 0 & 0 & 1 \end{bmatrix} \tag{3}$$

2.2 Model of Ship-to-Ship Interaction

Typically, the initial phase in formation control involves the establishment of the formation configura-

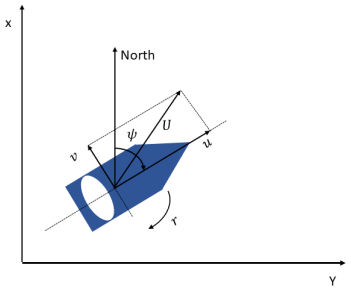

Figure 1: Three degrees of freedom motion model.

tion. For the purpose of facilitating the study of ship-to-ship interactions, the formations described in this paper are composed of two homogeneous ASVs, systematically categorized into three configurations as depicted in the Fig. 2, labeled as tandem, parallel and semi-triangle. The origin of the body-fixed coordinate system is set at mid-ship, and the $\vec{x}, \vec{y}, \vec{z}$ axis are point to the starboard, bow, and downwards, respectively. In the parallel formation (as shown in Fig. 2a) , the hull's bows are aligned, and the transverse separations is S_p without any longitudinal offset.In the Tandem formation (as shown in Fig. 2b), the longitudinal distances between the two ships is S_L, and the transverse offset is zero.The layout of the semi-triangle formation as shown in Fig. 2c. The parameters of the formation configurations in the subsequent calculations are presented in Table 1, where L and B represent the length and breadth of ship, respectively.

There are three main methods for studying hydrodynamic effects as mentioned in Section1. Although the accuracy of theoretical analysis and empirical model development is constrained, their capacity to offer rapid predictions and ease of application are critically valuable in real-time control. Consequently, this section will draw upon these methods and, by integrating formulas and data from the existing literature, will introduce a more universally applicable semi-empirical formula. Employing Vantorre's experimental results (Vantorre et al., 2002), Decker (De Decker, 2006) attempted to determine the applicability of Vantorre's results for lightering operations. The analysis employed regression techniques to focus on three dimensionless coefficients:C_X; C_Y *and* C_N, corresponding to surge, sway, and yaw movements, respectively. These coefficients are primarily influenced by the ships' longitudinal and lateral positions and their speeds, which can be described as follows:

$$C_X = \frac{X}{\frac{1}{2}\rho BTU_1U_2} \tag{4}$$

$$C_Y = \frac{Y}{\frac{1}{2}\rho LTU_1U_2} \tag{5}$$

$$C_N = \frac{N}{\frac{1}{2}\rho BLTU_1U_2}, \tag{6}$$

where B is the beam(m), T is the draught(m), U is the speed(m/s), L is the length(m), ρ is the water density. These formulas reveal that ship-ship interaction are predominantly governed by the speeds and relative positions of the two vessels. As the relative distance diminishes, the interactions begin to significantly intensify, a trend that is similarly observed with increasing vessel speeds.Furthermore, the presence of these interaction forces variably influences the maneuverability of the vessels.

For formation situations, He (He et al., 2022) Utilizing the Reynolds-Averaged Navier-Stokes (RANS) equations in conjunction with the $K-\omega$ turbulence models, a series of numerical simulations were conducted. The numerical simulation explores the relationship between ship resistance and formation configurations under various formation shapes, where these configurations primarily encompass the relative distance and speed of the ships. Subsequently, a third-order polynomial regression analysis was employed to derive the relationship between the resistance coefficient, relative position, and speed of the ships. The relationship of the follower ship under various formation shapes is shown as:

Tandem Formation:

$$\begin{aligned} X'_{Leader} &= -0.0118 + 6.3582 \times Fr^3 - 0.0017 \times S_L^3 \\ &\quad - 1.6286 \times Fr^2 + 0.0069 \times S_L^2 + 0.1680 \times Fr \\ &\quad - 0.0089 \times S_L + 0.0003 \times Fr \times S_L \end{aligned} \tag{7}$$

Parallel Formation:

$$\begin{aligned} X'_{Leader} &= -0.0191 + 9.0151 \times Fr^3 + 0.0011 \times S_P^3 \\ &\quad - 2.2171 \times Fr^2 - 0.0035 \times S_P^2 + 0.2206 \times Fr \\ &\quad + 0.0044 \times S_P - 0.0071 \times Fr \times S_P \end{aligned} \tag{8}$$

Triangle Formation:

$$\begin{aligned} X'_{Leader} &= -0.0093 + 6.0171 \times Fr^3 - 0.0001 \times S_P^3 \\ &\quad - 1.5498 \times Fr^2 + 0.0091 \times S_L^2 + 0.0005 \times S_P^2 \\ &\quad + 0.1604 \times Fr - 0.0139 \times S_L - 0.0029 \times S_P \\ &\quad + 0.0022 \times Fr \times S_L + 0.0009 \times Fr \times S_P \\ &\quad + 0.0044 \times S_L \times S_P, \end{aligned} \tag{9}$$

where Fr is the Froude Number,which can be expressed as:

$$Fr = \frac{V}{\sqrt{gL}}. \tag{10}$$

From these formulas, it can be inferred that across all formation types, ship resistance demonstrates a fundamentally linear and positive correlation with speed, indicating that an increase in speed corresponds to a rise in the total resistance coefficient. In tandem and parallel formation shapes, when the speed remains constant, the resistance coefficient is influenced by the lateral or longitudinal distances. In the case of the triangle formation, the relative distance encompasses both lateral and longitudinal dimensions, making its expression overly complex. Therefore, we usually assume a constant speed in the equations to ensure that the influencing factors are limited to two dimensions.

Owing to the unique characteristics of hydrodynamics, the follower ship is more susceptible to the

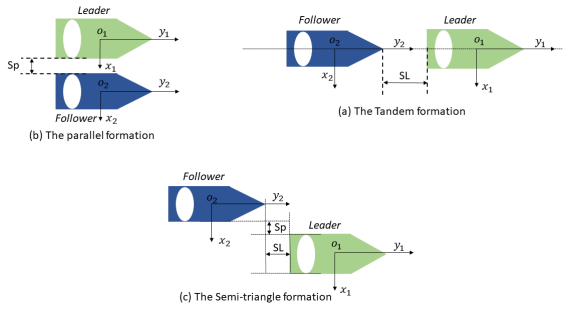

Figure 2: The geometric configuration of formation.

wake and wave effects generated by the leader. Therefore, this paper primarily concentrates on the follower ship and provides a comprehensive summary of the resistance formulas applicable in various scenarios. Given that total hull resistance is a function of hull form, ship speed, and water properties, the coefficient of total hull resistance similarly depends on these factors. The coefficient of total hull resistance is determined by the following equation:

$$X_T = \frac{R_T}{\frac{1}{2}\rho S v^2}, \tag{11}$$

where R_T is the total hull resistance and s is the wetted surface area of the underwater hull, ρ is the water density.

Based on equations (7) to (11), the three degrees of freedom ship-to-ship interaction forces for the follower ship can be expressed as follows:

$$\tau_s = \frac{1}{2}\rho\, S v^2 \left(\gamma v + \alpha L + \beta B + \varepsilon\right), \tag{12}$$

where $\tau_s = \left[\tau_{s_x}\ \tau_{s_y}\ \tau_{s_r}\right]^T$ represent the interaction forces and moments of three degrees of freedom respectively. $\gamma = \left[a_1\ a_2\ a_3\right]^T$ is the velocity parameters in the three degrees of freedom. $L = \left[SL^3\ SL^2\ SL\right]^T$ and $B = \left[SP^3\ SP^2\ SP\right]^T$. The terms $\alpha \in \mathbb{R}^{3\times3}$, $\beta \in \mathbb{R}^{3\times3}$ are longitudinal distance weights matrix and transverse separations weights matrix, respectively, which is defined as:

$$\alpha = \begin{bmatrix} \alpha_{11} & \alpha_{12} & \alpha_{13} \\ \alpha_{21} & \alpha_{22} & \alpha_{23} \\ \alpha_{31} & \alpha_{32} & \alpha_{33} \end{bmatrix}, \beta = \begin{bmatrix} \beta_{11} & \beta_{12} & \beta_{13} \\ \beta_{21} & \beta_{22} & \beta_{23} \\ \beta_{31} & \beta_{32} & \beta_{33} \end{bmatrix} \tag{13}$$

Table 1: Parameters of the formation configurations.

Formation shape	Relative distance	Velocity (m/s)
Single ASV	–	0.1–0.4
Tandem formation	0.1–2.0L	0.1–0.4
Parallel Formation	0.1–1.5B	0.1–0.4
Semi-Triangle	0.1–2.0L, 0.1–1.5B	0.1–0.4

3 SIMULATION EXPERIMENT DESIGN

In this section, we design simulation experiments for a formation composed of two homogeneous ASVs, introducing the parameter settings and experimental setup. Considering that the main influencing factors of ship-to-ship interaction are speed and relative distance, and that formation control also needs to manage speed and distance, we have designed two sets of experiments. These experiments separately consider the impact of variations in speed and distance on formation control.

3.1 Parameter Setup

Considering that acquiring hydrodynamic parameters for ships is often an extremely tedious process, this section applies the "Tito-Neri", which is developed by Delft University of Technology(TU Delft). "Tito-Neri" is a 1:30 replica model tugboat (Bruggink et al., 2018). The hydrodynamic model parameters of "Tito-Neri" are shown in Table 2.

Table 2: Parameters of the Tito-Neri.

Parameters	**Value**	**Parameters**	**Value**
m	16.9	$Y_{\dot{v}}$	-49.2
I_z	0.51L	$Y_{\dot{r}}$	0.0
x_g	0.0	$N_{\dot{v}}$	0.0
$X_{\dot{u}}$	-1.2	$N_{\dot{r}}$	-1.8

It can be observed that the parameters in the mass (M) and Coriolis-Centripetal (C) matrices are identified, but the damping matrix (D) is not acquired. The Tito-Neri replace the whole damping part $D(v_t)v(t)$ to the drag forces vector $\tau_{drag}(t)$:

$$\tau_{drag(t)} = \begin{bmatrix} \tau_{drag/u(\varphi_{(t)}\ ,\ u(t))} \\ \tau_{drag/v(\varphi_{(t)}\ ,\ v(t))} \\ \tau_{drag/r(r(t))} \end{bmatrix}, \tag{14}$$

where $\tau_{drag/u}$, $\tau_{drag/v}$ and $\tau_{drag/r}$ represent the drag forces and moment in x , y and z direction. The polynomial functions in x and y direction are determined by the velocity in the corresponding direction and heading angles. The polynomial function in z direction is calculated by the yaw velocity.

Based on the data presented in the report (Bruggink et al., 2018),which is shown as Fig. 3. We employed third-order polynomial regression analysis to derive regression functions for the x and y directions. velocities ranging from $0-0.4(m/s)$ and angles from

$0-1(\pi)$. The derived functions are as follows:

$$\begin{aligned}\tau_{drag/u} = & -0.1849+0.5327\times V(t)+0.8117\times\varphi(t)\\ & +0.5387\times v(t)^2-0.0784\times\varphi(t)^2\\ & +6.3668\times v(t)^3-0.7143\times\varphi(t)^3 \qquad (15)\\ \tau_{drag/v} = & -0.0348+0.1416\times v(t)+0.2760\times\varphi(t)\\ & +0.4710\times v(t)^2-0.5299\times\varphi(t)^2\\ & +0.9844\times v(t)^3+0.2930\times\varphi(t)^3\\ & -0.1159\times v(t)\times\varphi(t) \qquad (16)\end{aligned}$$

The simulation in the next section will conduct path following control for the follower ship based on this motion model. In path following, controlling the ship's speed (e.g., maintaining a constant velocity) enables the prediction of the target position the ship can attain at a future time. Since the focus of this paper is on investigating the impact of ship-to-ship interaction on control performance, a simple and easy-to-implement PID controller will be used. For a simple PID control system , the transfer function of PID controller is shown as:

$$u(t)=k_p e(t)+k_I\int e(t)dt\ +\ k_D\frac{de_t}{dt} \qquad (17)$$

3.2 Simulation Experiment Design

According to (12), the main influencing factors of ship-to-ship interaction forces are velocity and relative distance. Therefore, this section will study their impact on control performance based on different geometric configurations. The simulation experiments will be divided into velocity experiments and distance experiments: In the velocity experiments, the initial distance between the two ASVs is set at the minimum and is maintained consistently. Then, the speeds of the two ships are precisely controlled to achieve the desired values. After completing a set of experiments, the initial distance is increased until it reaches twice the ship length, The process of velocity simulation is as shown in the Fig 4a; Similarly, for the distance experiments, the initial set maintains a constant desired speed of 0.1 m/s for both ASVs. Then, the distance between the two ships is gradually reduced from twice the ship length to 0.1 times the ship length. After completing this set of experiments, the desired speed of the two ships is increased until the desired speed reaches 0.3 m/s, as shown in the Fig 4b. The specific simulation parameters are as follows:

- In speed experiments, the two ships are in a tandem formation with an initial relative distance of SL_k. The initial positions and speeds of the two ships: $y_{leader}=(1,SL_k)$, $y_{follower}=(1,0)$, $v=(u_0,v_0,r_0)=(0,0,0)$, Desired Speed $v_d=0.01i\,(i=1,2,\ldots)$.
- In distance experiment, the initial speed is v_j , the initial positions of the two ships are: $y_{leader}=(1,2L)$, $y_{follower}=(1,0)$, and the desired relative distance is $SL_i=2L-0.01iL\,(i=1,2,\ldots)$.

4 SIMULATION RESULTS AND DISCUSSION

This section begins with simple simulation experiments to verify the feasibility of the follower ship controller. In this simulation, ship-to-ship interaction forces are ignored, focusing only on the follower ship's ability to follow the leader ship. Subsequently, velocity and distance simulations are conducted separately. These simulations focus on the impact of ship-to-ship interaction forces on control, recording the follower ship's relevant data to analyze how changes in these two factors affect the results. The settings for the controller test simulations are as follows: The initial position of the follower ship is located at the $(0,1)$ with 0 degree of heading and no speed, the leader ship is $y_{leader}=(1,0)$ with no speed. The desired distance is $1m$. The simulation results for the follower ship are presented as fig. 5. From the simulation results, it shows that when ship-to-ship interaction are not considered, the follower ship is able to track the leader ship well and maintain the desired distance.

The velocity simulation experiments and distance simulation experiments in this section are both based on the following assumptions:

- Assumption 1: This study concentrates on the control dynamics of the trailing ship under the influence of ship-to-ship interactions.Consequently, it is assumed that the leader ship adheres precisely to the predetermined trajectory, unaffected by ship-to-ship interactions.
- Assumption 2: In tandem formations, given that the centers of the two ships are perfectly aligned, it is posited that the ship-to-ship interactions are negligible in the Y and Z directions. So the 12 can be set as follow:

$$\begin{aligned}&\tau_s=[\tau_x,0,0]^T\\ &\tau_x=\frac{1}{2}\rho S v^2\left(a_1\times v+\alpha_{11}SL^3+\alpha_{12}SL^2+\alpha_{13}SL+\varepsilon\right)\\ &v(t)\in[0,v_{max}]\\ &SL\in[0.1L,2L]\end{aligned} \qquad (18)$$

4.1 Velocity Simulation

The velocity experiment is structured into 20 distinct groups, with the distance between the two ships incrementally increasing from 0.1 to 2 times the ship

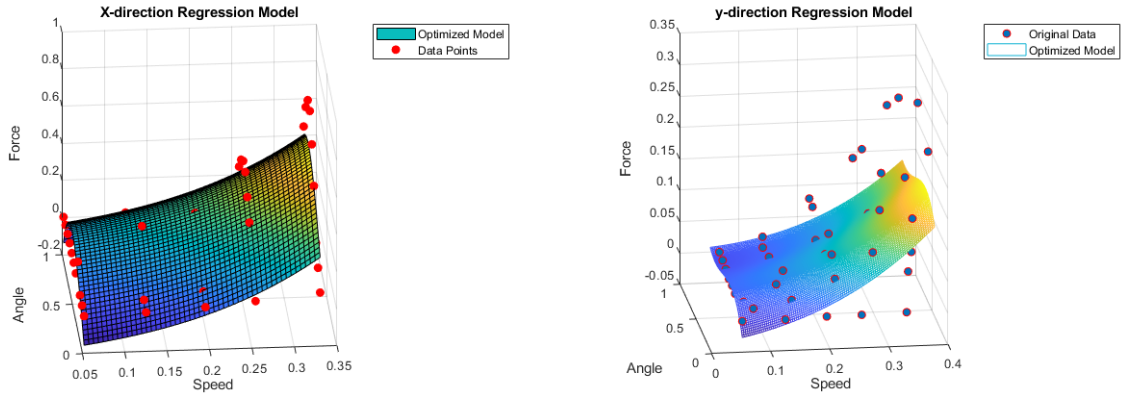

(a) x-direction. (b) y-direction.

Figure 3: Corresponding fitting surface of drag forces.

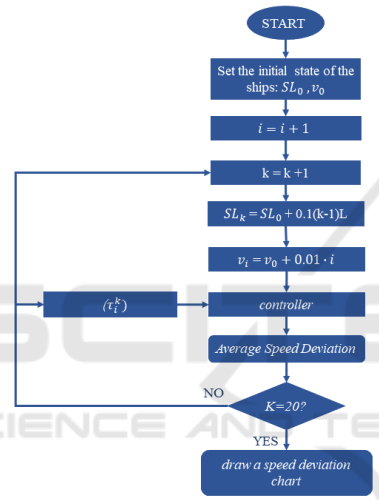

(a) The flowchart of velocity simulation.

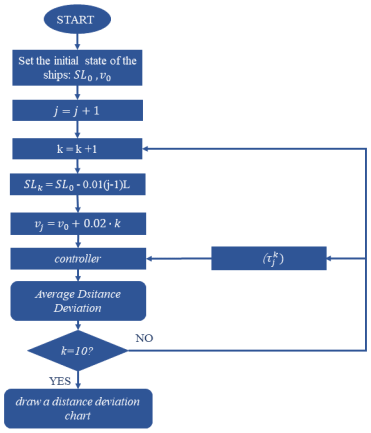

(b) The flowchart of distance simulation.

Figure 4: The flowchart of Simulation.

length in each group. It is hypothesized that the interaction between the two ships varies solely based on the velocity of the follower ship.The simulation results, which display the velocity variations and velocity errors of the trailing ship across each group, are illustrated in the below.

The simulation results delineate the performance at distances of $0.1L$, $1L$, and $2L$, shown as fig. 6 to fig. 8 with additional results presented in the accompanying table. The simulation outcomes clearly demonstrate that the interaction forces between the ships significantly impact the performance of the controller. For the Follower ship, observable fluctuations in speed and the emergence of a steady-state error are documented, as illustrated in Fig. 7a. This finding underscores that a solitary PID controller is inadequate to effectively counteract the complex effects induced by the interaction forces between ships. As the initial relative distance incrementally increases, the average speed error initially escalates and subsequently subsides. As delineated in Table 3, the error rate peaks when the relative distance reaches 1.2L. This phenomenon is attributed to the influence of the initial relative distance; the equation reveals that at a distance of 1.2L, the force exerted on the trailing ship maximizes before beginning to wane. Fig. 7d illustrates that the interaction force between the ships is positively correlated with speed and exhibits significant sensitivity to speed variations.

4.2 Distance Simulation

In the distance experiment, ten distinct trial groups will be conducted. The initial expected speed for the experiments will incrementally increase from 0.1 m/s to 0.3 m/s. In each experimental group, the distance between the two ships will be systematically reduced to investigate changes in interaction forces and their

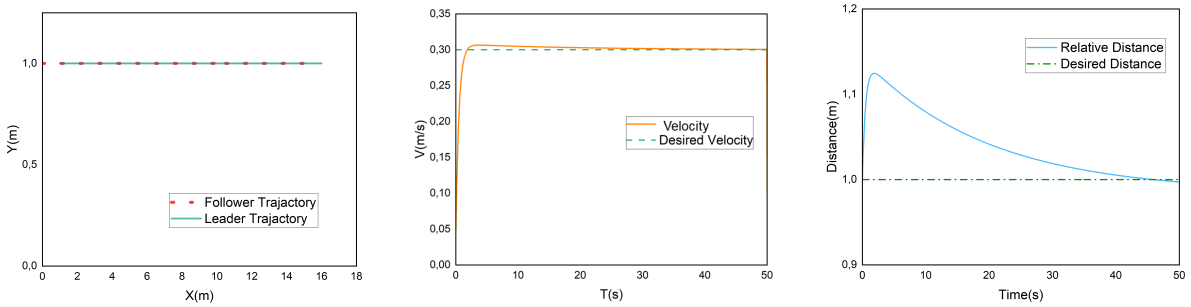

(a) Path following. (b) Velocity. (c) Relative Distance.

Figure 5: Simulation test results Without considering Ship-to-Ship Interaction.

Table 3: The velocity errors of Velocity Experiments.

Longitudinal distances (SL)	Average Velocity errors E_v (m/s)	Average Error rate D_v (%)
0.1L	0.0110	3.84
0.2L	0.0124	4.66
0.3L	0.0165	5.33
0.4L	0.0197	5.95
0.5L	0.0212	6.44
0.6L	0.0224	6.96
0.7L	0.0251	7.74
0.8L	0.0265	8.32
0.9L	0.0271	8.93
1.0L	0.0279	9.95
1.1L	0.0297	10.51
1.2L	0.0345	11.56
1.3L	0.0376	10.01
1.4L	0.0274	8.81
1.5L	0.0245	8.16
1.6L	0.0224	7.05
1.7L	0.0188	5.85
1.8L	0.0156	5.27
1.9L	0.0102	4.58
2.0L	0.0115	3.96

effects on control performance. The average distance error and average error rate for the experiments are presented in Table 4. The overall trend indicates that as the speed increases, the error correspondingly increases. This suggests that the increase in expected speed results in a heightened maximum interaction force between the ships, thereby exerting a more substantial impact on control.

Fig. 9 through 11 display the simulation outcomes for the follower ship at expected speeds of 0.1, 0.2, and 0.3 m/s, respectively. From Fig 9b, it is evident that an increase in expected speed correlates with a rise in the maximum value of the distance error. Fig 9c illustrates that during the interval between 20 and 40 seconds, there are pronounced speed fluctuations. During this interval, with the distance between the two ships ranging from 1.5L to 0.5L, it is indicated that distance exerts a significant influence on ship control. Fig. 9d delineates the trend of interaction forces between the ships relative to distance; however, overall, the influence of distance remains comparatively minor. In contrast, higher expected speeds result in increased overall forces exerted on the trailing ship, demonstrating that speed plays a more substantial role in influencing interaction forces between the ships than distance does.

Table 4: Distance Error of Distance experiments.

Velocity (m/s)	Average Distance Deviation Rate D_L (%)	Average Distance Error (m)
0.10	1.177	0.0154
0.12	1.385	0.0181
0.14	1.592	0.0202
0.16	1.774	0.0246
0.18	2.012	0.028
0.20	2.234	0.0305
0.22	2.382	0.0331
0.24	2.557	0.0367
0.26	2.831	0.039
0.28	3.157	0.0414
0.30	3.406	0.0452

5 CONCLUSIONS AND FURTHER RESEARCH

This paper addresses the frequently overlooked effects of ship-to-ship interactions in formation control. In scenarios where ships operate in close proximity, the interaction forces between them play a pivotal role. Consequently, this paper first proposes a semi-empirical formula for ship-to-ship interaction, followed by conducting pertinent formation control experiments using the Tito-Neri vessel which is developed by TU Delft.

The semi-empirical formula precisely delineates the primary factors influencing ship-to-ship interaction, specifically the relative positions and velocities of the two ships. Consequently, this study designs two experimental sets to systematically explore the effects of position and velocity, respectively, recording the simulation outcomes for the follower ship. However, when accounting for the interaction between the two ships, the overall control performance of the trailing ship deteriorates significantly. Speed fluctuations not only occur but also precipitate the emergence of steady-state errors. This is attributed to speed being the principal factor influencing the interaction force, which functions as an external disturbance and significantly impacts the control of the trailing ship. Simulation results reveal that as speed increases, the interaction force between the two ships intensifies, thereby amplifying its impact on control.

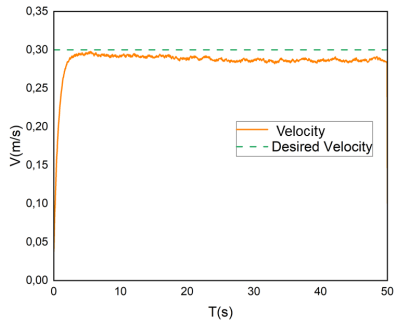

(a) Velocity.

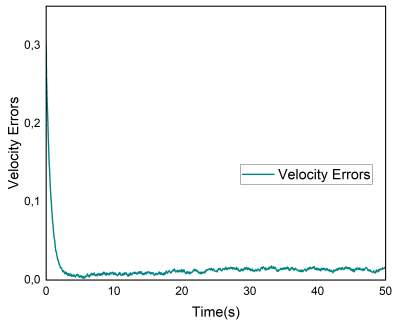

(b) Velocity errors.

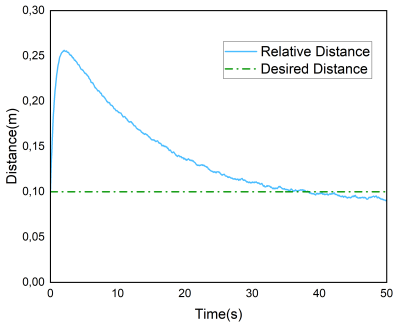

(c) Relative Distances.

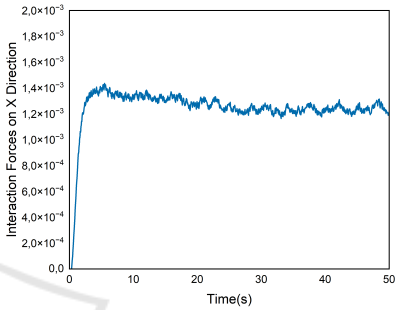

(d) Forces on X Direction.

Figure 6: Simulation of 0.1L distance.

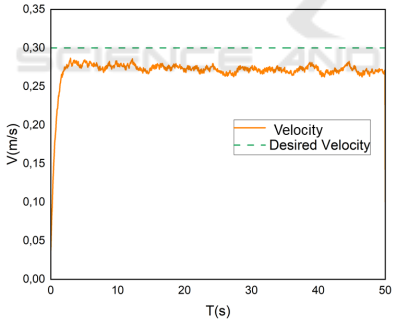

(a) Velocity.

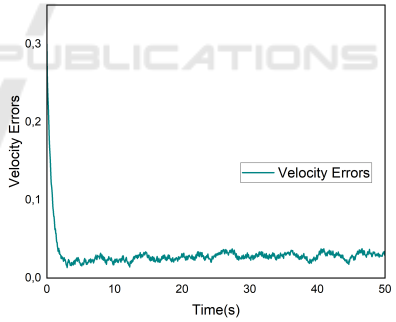

(b) Velocity errors.

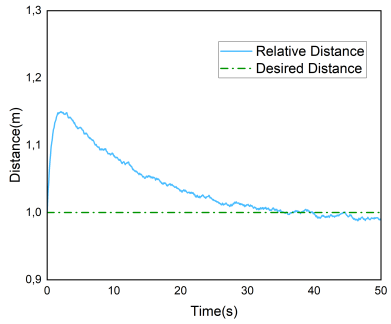

(c) Relative Distances.

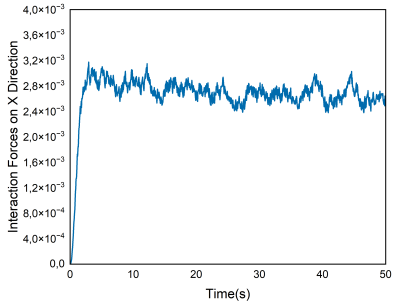

(d) Forces on X Direction.

Figure 7: Simulation of 1L distance.

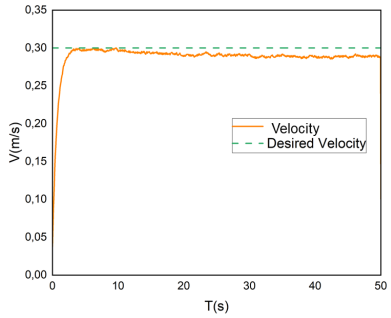

(a) Velocity.

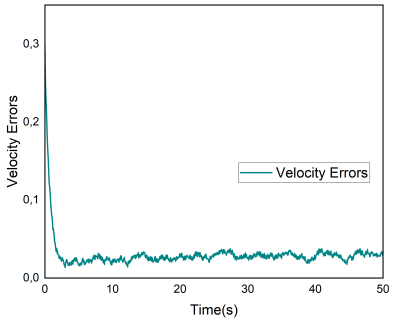

(b) Velocity errors.

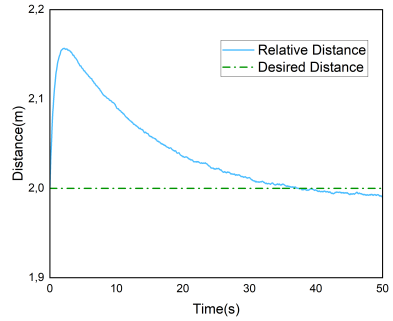

(c) Relative Distances.

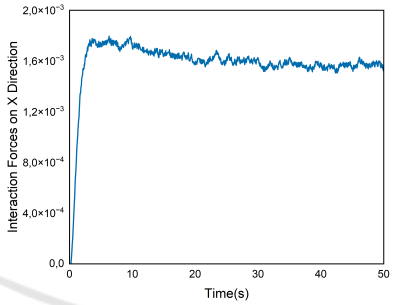

(d) Forces on X Direction.

Figure 8: Simulation of 2L distance.

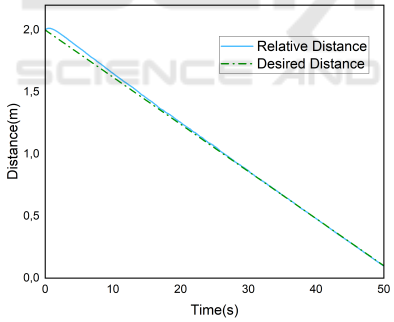

(a) Distance.

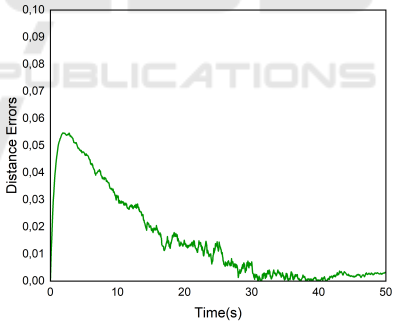

(b) Distance errors.

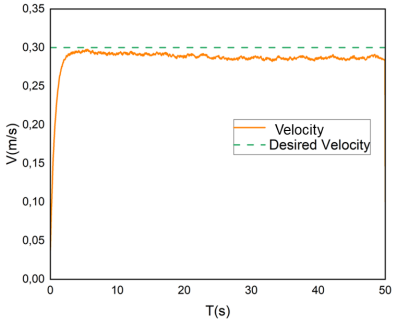

(c) Velocity.

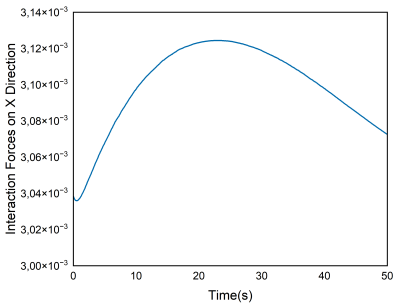

(d) Forces on X Direction.

Figure 9: Simulation of 0.1m/s.

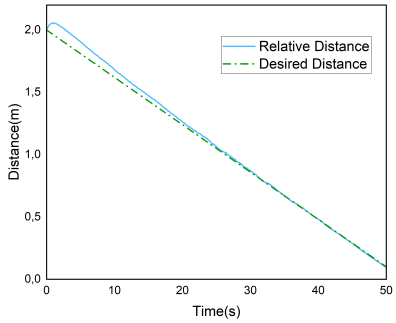

(a) Distance.

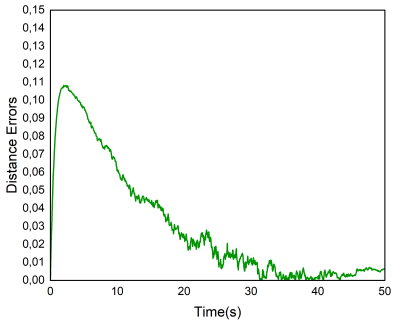

(b) Distance errors.

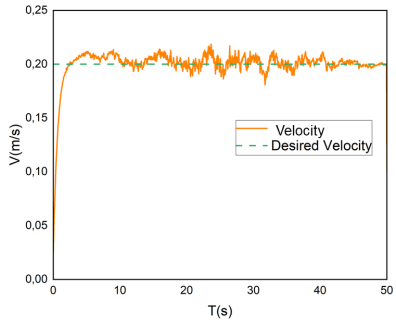

(c) Velocity.

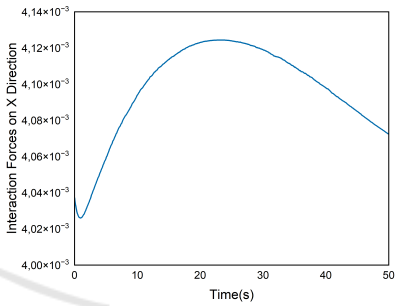

(d) Forces on X Direction.

Figure 10: Simulation of 0.2m/s.

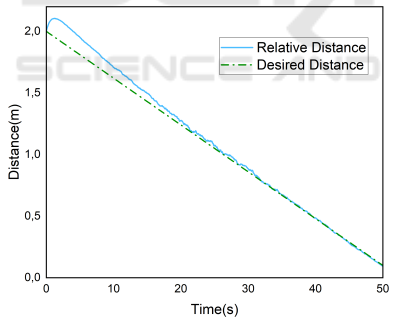

(a) Distance.

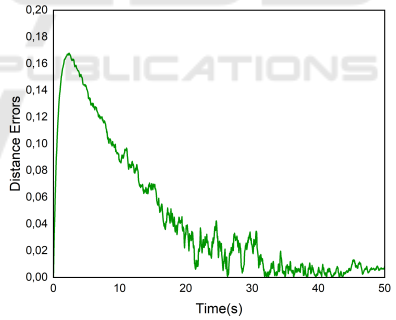

(b) Distance errors.

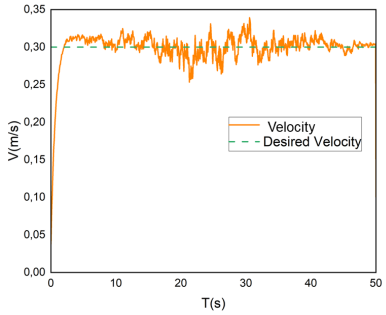

(c) Velocity.

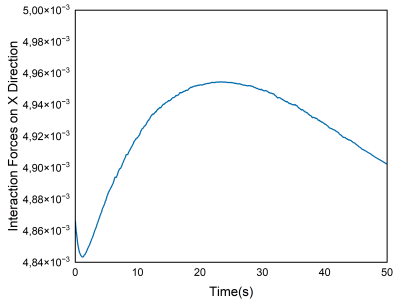

(d) Forces on X Direction.

Figure 11: Simulation of 0.3m/s.

Concerning distance, while the relative distance exerts a lesser impact on control performance compared to speed, it still markedly influences the control performance of the follower ship within the range of 1 to 1.2 times the ship's length. Within this range, speed fluctuations are particularly pronounced. Overall, the interaction force between the two ships is governed by both speed and distance, demonstrating greater sensitivity to changes in speed. If these variations in force are not incorporated into the controller design, they could readily result in degraded control performance or even failure.

The current study exclusively investigates a scenario involving two ships in tandem and is designed to visually demonstrate the impact of ship-to-ship interaction forces on control. Controllers are specifically tailored for the follower ship, with the tracking path constrained to straight lines. Future research will broaden the scope of experimental scenarios to encompass various formation configurations, incorporating the interaction forces among ships within these formations. Additionally, to verify the impact of ship-to-ship interaction forces on control, this paper employed a relatively simple PID controller. This type of controller has poor robustness and struggles to account for the inherent limitations of ASV, such as rudder angle rate and thruster output. Therefore, it is necessary to design a more suitable controller specifically tailored to these conditions to ensure the performance of the control system.

ACKNOWLEDGMENTS

This research is supported by the "Researchlab Autonomous Shipping (RAS)" of Delft University of Technology.

REFERENCES

Bruggink, D., Cremer, Q., Groenewegen, R., and Klokgieters, A. (2018). Differentiation of maneuvering coefficients for scaled model vessels. Technical report, Technical report, Delft University of Technology.

Chen, C.-W., Chen, Y., and Cai, Q.-W. (2019). Hydrodynamic-interaction analysis of an autonomous underwater hovering vehicle and ship with wave effects. *Symmetry*, 11(10):1213.

Chen, L., Negenborn, R. R., Huang, Y., and Hopman, H. (2021). Survey on cooperative control for waterborne transport. *IEEE Intelligent Transportation Systems Magazine*, 13(2):71–90.

De Decker, B. (2006). *Ship-ship interaction during lightering operations*. PhD thesis, MSc. thesis, NTNU, Trondheim Norway.

Dong, Z., Liang, X., Guan, X., and Li, W. (2022). Formation optimization of various spacing configurations for a fleet of unmanned surface vehicles based on a hydrodynamic energy-saving strategy. *Ocean Engineering*, 266:112824.

Du, Z., Negenborn, R. R., and Reppa, V. (2021a). Cooperative multi-agent control for autonomous ship towing under environmental disturbances. *IEEE/CAA Journal of Automatica Sinica*, 8(8):1365–1379.

Du, Z., Negenborn, R. R., and Reppa, V. (2021b). Cooperative multi-agent control for autonomous ship towing under environmental disturbances. *IEEE/CAA Journal of Automatica Sinica*, 8(8):1365–1379.

Fossen, T. I. (2011). *Handbook of marine craft hydrodynamics and motion control*. John Wiley & Sons.

Gu, N., Wang, D., Peng, Z., and Liu, L. (2019). Observer-based finite-time control for distributed path maneuvering of underactuated unmanned surface vehicles with collision avoidance and connectivity preservation. *IEEE Transactions on Systems, Man, and Cybernetics: Systems*, 51(8):5105–5115.

He, S., Wang, M., Dai, S.-L., and Luo, F. (2019). Leader–follower formation control of usvs with prescribed performance and collision avoidance. *IEEE Transactions on Industrial Informatics*, 15(1):572–581.

He, Y., Mou, J., Chen, L., Zeng, Q., Chen, P., and Zhang, S. (2021). Survey on hydrodynamic effects on cooperative control of maritime autonomous surface ships. *Ocean Engineering*, 235:109300.

He, Y., Mou, J., Chen, L., Zeng, Q., Huang, Y., Chen, P., and Zhang, S. (2022). Will sailing in formation reduce energy consumption? numerical prediction of resistance for ships in different formation configurations. *Applied Energy*, 312:118695.

Lataire, E., Vantorre, M., and Delefortrie, G. (2009). Captive model testing for ship to ship operations. In *International Conference on Marine Simulation and Ship Maneuverability (MARSIM'09)*. Panama Canal Authoritiy; International Marine Simulator Forum.

Lataire, E., Vantorre, M., Vandenbroucke, J., and Eloot, K. (2011). Ship to ship interaction forces during lightering operations. In *2nd International conference on Ship Manoeuvring in Shallow and Confined Water: Ship to ship interaction*, pages 211–222. Royal Institution of Naval Architects.

Liu, L., Wang, D., Peng, Z., and Li, T. (2017). Modular adaptive control for los-based cooperative path maneuvering of multiple underactuated autonomous surface vehicles. *IEEE Transactions on Systems, Man, and Cybernetics: Systems*, 47(7):1613–1624.

Liu, L., Wang, D., Peng, Z., Li, T., and Chen, C. P. (2018). Cooperative path following ring-networked under-actuated autonomous surface vehicles: Algorithms and experimental results. *IEEE transactions on Cybernetics*, 50(4):1519–1529.

Liu, L., Xu, Y., Huang, Z., Wang, H., and Wang, A. (2022). Safe cooperative path following with relative-angle-based collision avoidance for multiple underactuated autonomous surface vehicles. *Ocean Engineering*, 258:111670.

Liu, Y., Liu, J., He, Z., Li, Z., Zhang, Q., and Ding, Z. (2023). A survey of multi-agent systems on distributed formation control. *Unmanned Systems*, 0(0):1–14.

Mondal, A., Behera, L., Sahoo, S. R., and Shukla, A. (2017). A novel multi-agent formation control law with collision avoidance. *IEEE/CAA Journal of Automatica Sinica*, 4(3):558–568.

Mu, D. D., Wang, G. F., and Fan, Y. S. (2020). Formation control strategy for underactuated unmanned surface vehicles subject to unknown dynamics and external disturbances with input saturation. *International Journal of Control, Automation and Systems*, 18(11):2742–2752.

Negenborn, R. R., Goerlandt, F., Johansen, T. A., Slaets, P., Valdez Banda, O. A., Vanelslander, T., and Ventikos, N. P. (2023). Autonomous ships are on the horizon: here's what we need to know. *Nature*, 615(7950):30–33.

Oh, K.-K., Park, M.-C., and Ahn, H.-S. (2015). A survey of multi-agent formation control. *Automatica*, 53:424–440.

Park, B. S. and Yoo, S. J. (2018). An error transformation approach for connectivity-preserving and collision-avoiding formation tracking of networked uncertain underactuated surface vessels. *IEEE transactions on cybernetics*, 49(8):2955–2966.

Peng, Z., Jiang, Y., and Wang, J. (2020a). Event-triggered dynamic surface control of an underactuated autonomous surface vehicle for target enclosing. *IEEE Transactions on Industrial Electronics*, 68(4):3402–3412.

Peng, Z., Wang, J., Wang, D., and Han, Q.-L. (2020b). An overview of recent advances in coordinated control of multiple autonomous surface vehicles. *IEEE Transactions on Industrial Informatics*, 17(2):732–745.

Qin, Z., Lin, Z., Yang, D., and Li, P. (2017). A task-based hierarchical control strategy for autonomous motion of an unmanned surface vehicle swarm. *Applied Ocean Research*, 65:251–261.

Sano, M. and Yasukawa, H. (2019). Simulation study of approach manoeuvre in lightering and reverse lightering operations. *Ocean Engineering*, 187:106185.

Setiawan, H. and Muin, M. (2018). Dynamic response of breasting dolphin moored with 40,000 dwt ship due to parallel passing ship phenomenon. In *MATEC Web of Conferences*, volume 147, page 05003. EDP Sciences.

Skjetne, R., Smogeli, Ø. N., and Fossen, T. I. (2004). A nonlinear ship manoeuvering model: Identification and adaptive control with experiments for a model ship.

Tan, G., Zhuang, J., Zou, J., and Wan, L. (2023). Adaptive adjustable fast marching square method based path planning for the swarm of heterogeneous unmanned surface vehicles (usvs). *Ocean Engineering*, 268:113432.

Vantorre, M., Verzhbitskaya, E., and Laforce, E. (2002). Model test based formulations of ship-ship interaction forces. *Ship Technology Research*, 49:124–141.

Varyani, K., McGregor, R., Krishnankutty, P., and Thavalingam, A. (2002). New empirical and generic models to predict interaction forces for several ships in encounter and overtaking manoeuvres in a channel. *International shipbuilding progress*, 49(4):237–262.

Wang, H., Luo, Q., Li, N., and Zheng, W. (2022). Data-driven model free formation control for multi-usv system in complex marine environments. *International Journal of Control, Automation and Systems*, 20(11):3666–3677.

Wnęk, A., Sutulo, S., and Guedes Soares, C. (2018). Cfd analysis of ship-to-ship hydrodynamic interaction. *Journal of Marine Science and Application*, 17:21–37.

Xiong, G., Zhu, F., Liu, X., Dong, X., Huang, W., Chen, S., and Zhao, K. (2015). Cyber-physical-social system in intelligent transportation. *IEEE/CAA Journal of Automatica Sinica*, 2(3):320–333.

Yu, D., Wang, L., and Yeung, R. W. (2019). Experimental and numerical study of ship-to-ship interactions in overtaking manoeuvres. *Proceedings of the Royal Society A*, 475(2225):20180748.

Yuan, Z.-M., Ji, C.-Y., Incecik, A., Zhao, W., and Day, A. (2016). Theoretical and numerical estimation of ship-to-ship hydrodynamic interaction effects. *Ocean Engineering*, 121:239–253.

Zhou, W., Wang, Y., Ahn, C. K., Cheng, J., and Chen, C. (2020). Adaptive fuzzy backstepping-based formation control of unmanned surface vehicles with unknown model nonlinearity and actuator saturation. *IEEE Transactions on Vehicular Technology*, 69(12):14749–14764.